

Flexural Strength and Ductility of Extended Pile-Shafts. II: Experimental Study

Y. H. Chai, M.ASCE,¹ and Tara C. Hutchinson, M.ASCE²

Abstract: Results of an experimental program investigating the lateral strength and ductility capacity of reinforced concrete piles are presented. Four full-scale reinforced concrete piles with details representative of the current California design were tested under combined axial compression and reversed cyclic lateral displacement. Test parameters include confining steel ratio, aboveground height, and soil density. Of particular interests are the lateral strength and stiffness of the soil-pile system, depth-to-maximum-moment, and magnitude of local deformation upon formation of a plastic hinge in the pile. Equivalent plastic hinge lengths were determined using curvatures measured along the length of the pile. Test results indicated that the equivalent plastic hinge length of piles is generally longer than that of an equivalent base-restrained column. The equivalent plastic hinge length of the pile depends primarily on the aboveground height of the pile, but is not overly sensitive to the soil density. Test results also provided the basis for an analytical model presented in a companion paper for assessing the local ductility demand of a yielding pile-shaft.

DOI: 10.1061/(ASCE)0733-9445(2002)128:5(595)

CE Database keywords: Flexural strength; Ductility; Concrete piles; Concrete, reinforced; Experimentation.

Introduction

Seismic performance of a bridge structure depends on the ductility capacity of its yielding members. For bridge structures supported on extended pile-shafts, yielding may occur in the pile at some distance below the ground level. In the case of reinforced concrete piles, the overall ductility capacity of the structure depends on the local ductility capacity of the pile, which must be adequately confined to ensure a ductile behavior. Although requirements for transverse reinforcement in concrete piles frequently follow that of reinforced concrete columns, the distribution of bending moment in the pile is more gradual compared to that in an equivalent base-restrained column. This is due to the surrounding soil, which extends the zone of plasticity in the pile, and therefore provides a larger ductility capacity to the pile. In addition to a larger spread of curvature, the lateral restraint provided by the surrounding soil may also increase the ultimate compressive strain of the concrete, thereby increasing the ultimate curvature that can be tolerated by the pile.

Although analytical studies have shown that the equivalent plastic hinge length of concrete piles varies from one to two pile diameters depending on the soil stiffness and aboveground height (Priestley et al. 1996; Budek et al. 2000), very few tests have been performed to verify such results. Ductility capacity of reinforced or prestressed concrete piles is frequently assessed without

a soil medium with the pile loaded transversely in a statically determinate configuration (Sheppard 1983; Park and Falconer 1983; Banerjee et al. 1987; Budek 1997). A predetermined bending moment distribution, estimated from a soil-pile interaction analysis, is imposed on the pile to simulate the action of the soil on the pile. The actual interaction between the soil and pile, however, represents a highly indeterminate system with possible redistribution of bending moment upon yielding of the soil and pile. The predetermined bending moment, as commonly assumed for structural testing of piles, does not allow for such redistribution and may represent too severe of a condition for assessing the ductility capacity of the pile. This paper presents the results of a test program conducted on full-sized reinforced concrete piles embedded in a cohesionless soil. The test program was intended to provide the experimental basis for an analytical model presented in a companion paper (Chai 2002) for assessing the flexural strength and ductility capacity of an embedded pile. Particular emphasis of the testing was placed on characterization of the local inelastic deformation and the equivalent plastic hinge length of the pile.

Experimental Program

The experimental program consisted of lateral load testing of four full-scale (406 mm diameter) reinforced concrete piles embedded in two different soil conditions: loose dry sand and dense dry sand. In addition to the variation of soil density, aboveground heights of $6D$ and $2D$, where D =diameter of the pile, were tested to investigate the influence of the bending moment gradient on the pile curvature distribution and the associated plastic hinge length. Table 1 summarizes the main test parameters including the confining steel ratio of the test pile and density of the test soil.

Test Setup

Fig. 1 shows the test setup for the soil-pile interaction test. The test pile was embedded in a large soil container, which had a

¹ Associate Professor, Dept. of Civil and Environmental Engineering, Univ. of California, Davis, CA 95616.

² Assistant Professor, Dept. of Civil and Environmental Engineering, Univ. of California, Irvine, CA 92697-2175.

Note. Associate Editor: C. Dale Buckner. Discussion open until October 1, 2002. Separate discussions must be submitted for individual papers. To extend the closing date by one month, a written request must be filed with the ASCE Managing Editor. The manuscript for this paper was submitted for review and possible publication on June 6, 2000; approved on August 22, 2001. This paper is part of the *Journal of Structural Engineering*, Vol. 128, No. 5, May 1, 2002. ©ASCE, ISSN 0733-9445/2002/5-595-602/\$8.00+\$0.50 per page.

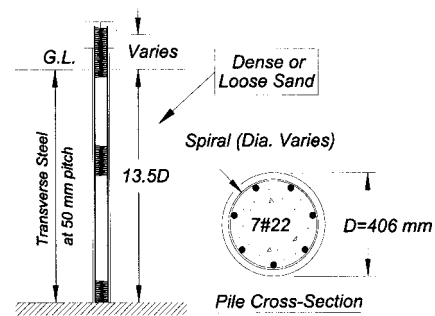
Table 1. Test Matrix

Pile No.	Aboveground height	Soil density	Confining steel ratio
1	2D	dense	0.57%
2	2D	loose	0.57%
3	6D	dense	1.06%
4	6D <td loose	1.06%	

diameter of 6.71 m and a depth of 5.49 m. The soil container was designed to have a radius larger than $6D$ between the pile and container wall in order to minimize the influence of the boundary wall on pile response (Park et al. 1987). The embedded length of the pile was $13.5D$, which was sufficiently long to develop an equivalent fixed-base cantilever response even in a loose soil condition. The axial compression on the pile was applied using two high-strength steel tie-down rods, each stressed by a centerhole hydraulic jack. The tie-down rods were allowed to move freely inside two vertical culverts on each side of the soil container. The axial force applied to the test piles was $P=445$ kN, corresponding to a nominal axial stress level of $0.1f'_c$, where f'_c =uniaxial compressive strength of concrete. The lateral force on the pile was provided by a long-stroke double-acting actuator reacting against a large-capacity reaction block.

Test Pile Details

Reinforcement details for the test pile were representative of the California Dept. of Transportation (Caltrans) current design for 620 kN (70 ton) piles, with the exception of the transverse reinforcement where the confinement ratio was varied. Fig. 2 shows the reinforcement details for the test pile, where the longitudinal reinforcement was provided by seven Grade A706 $\Phi 22$ bars ($d_b=22.2$ mm), representing a longitudinal reinforcement ratio of $\rho_l=2.1\%$. A clear cover of 50 mm was provided for the longitudinal reinforcement. The test pile was confined by a continuous spiral of MW25 or MW45 smooth wire ($d_{sp}=5.4$ or 7.3 mm, respectively) at 50 mm pitch. For the test pile with an aboveground height of $2D$, MW25 spiral was used to provide a confining steel ratio of $\rho_s=0.57\%$, or about one-half of that required by ATC-32 (1996). For the test pile with an aboveground height of $6D$, MW45 spiral was used to provide $\rho_s=1.06\%$, which was close to the confining steel ratio required by ATC-32 (1996).

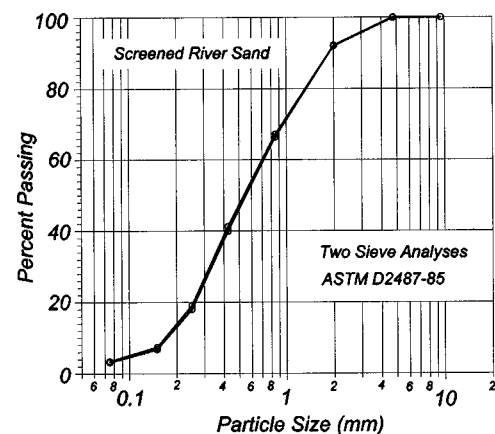
**Fig. 1.** Soil-pile interaction test setup**Fig. 2.** Reinforcement details for test piles

The stress-strain curve of the longitudinal steel was characterized by a well-defined yield stress of $f_y=421$ MPa, whereas the transverse steel did not have a well-defined yield stress. At 0.2% offset strain, the equivalent yield stress of the MW25 transverse steel was 710 MPa, while that of the MW45 transverse steel was slightly lower at about 605 MPa. Test piles were constructed in pairs resulting in the uniaxial compressive strength of the concrete being nearly equal for the pair of piles at the time of testing. For the first pair of piles with an aboveground height of $2D$ the compressive strength of the concrete was $f'_c=41$ MPa, whereas for the second pair of piles with an aboveground height of $6D$ the compressive strength was slightly higher with $f'_c=47.5$ MPa.

Test Soil Properties

A locally available river sand was used as the test soil. The particle size distribution, based on two sieve analyses of the test soil, is shown in Fig. 3. The median grain size was about 0.5 to 0.6 mm, the coefficient of uniformity was about 4.4, and the coefficient of curvature was about 0.9. The test soil can be classified as clean, poorly graded sand (SP) in accordance with the Unified Soil Classification System (USCS), with about 3% fines (% passing No. 200 sieve) and no gravel (0% retained on No. 4 sieve).

In terms of installation procedure, the test pile was inserted as a precast unit in the soil container before placement of the soil and was supported vertically by end-bearing on the base slab. For the dense sand condition, the soil was compacted in 150 mm lifts using a vibratory flat-plate compactor (weight between 1.8 and 1.6 kN) with three compaction passes per lift. For the loose sand condition, the soil was compacted in 230 mm lifts with a single

**Fig. 3.** Particle size distribution for test soil

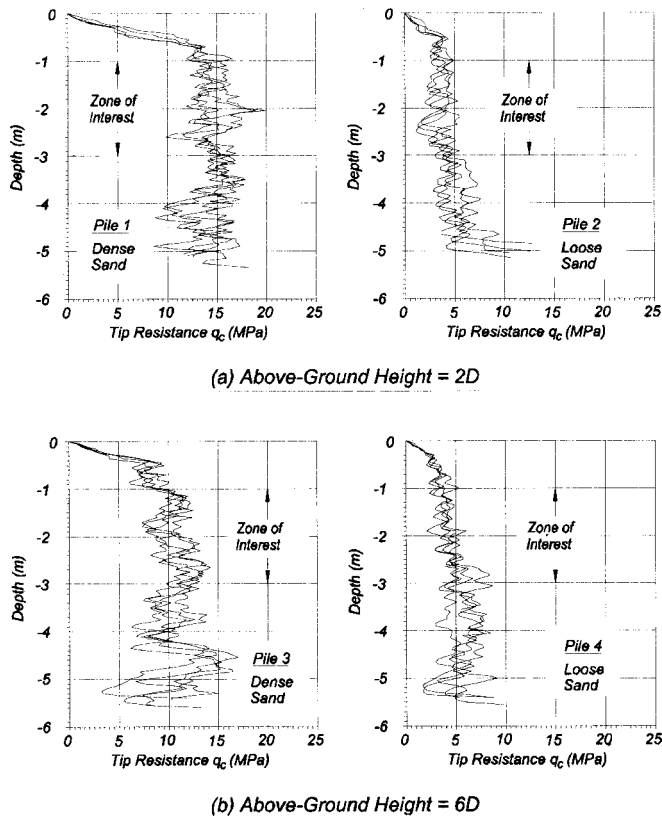


Fig. 4. Measured cone penetrometer tests tip resistances

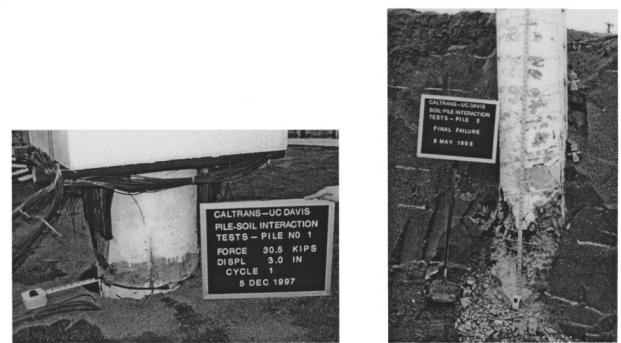
pass per lift. Density and moisture content were measured at every other lift using a nuclear density gage to ensure a uniform compaction of the soil. For the dense sand, average wet densities over the full depth of the container were 18.0 and 18.2 kN/m³ for the pile with above heights of 2D and 6D, respectively. For the loose sand, average wet densities were similar for both above-ground heights at 17.0 kN/m³. The in-place moisture content generally varied between 5 and 8% for the four tests.

The in-place mechanical properties of the soil were characterized by cone penetrometer tests (CPT) and shear wave velocity soundings. Four CPT soundings were taken per pile at locations near midway between the test pile and wall of the container. Fig. 4 shows the variation of the measured tip resistance, q_c , with depth for all four pile tests. The average tip resistance was fairly uniform with depth and had values of approximately 14.6 and 10.8 MPa for the dense sand and 3.6 and 4.5 MPa for the loose sand. To correct for the influence of overburden pressure on the measured tip resistance, the tip resistance q_c was normalized using the Liao and Whitman (1986) procedure. The normalized tip resistance is given by $q_{c1} = C_N q_c$, where $C_N = \sqrt{P_a / \sigma'_v}$ with reference pressure $P_a = 0.1$ MPa, σ'_v = effective overburden pressure, and C_N limited to a maximum value of 2.0. In the upper 1–3 m, the normalized tip resistance q_{c1} averaged 25 and 18 MPa for the piles in dense sand and approximately 6 and 7 MPa for the piles in loose sand. Using these normalized tip resistances, friction angles of the test soil were estimated to be $\bar{\phi} = 44^\circ$ and 42° for the dense sand and $\bar{\phi} = 37^\circ$ and 38° for the loose sand (Mair and Wood 1987). Based on the average value of the corrected tip resistance, relative densities of the in-place sand, D_r , were estimated to be 94% and 84% for the dense condition (first and third piles), and 53% and 59% for the loose condition (second and fourth piles) (Meyerhof 1956).

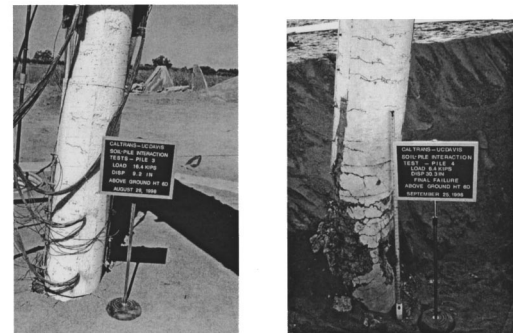
Table 2. Summary of In-Place Sand Properties

Pile No.	q_c (MPa)	q_{c1} (MPa)	D_r (%)	$\bar{\phi}$ (deg)	v_s (m/s)	v_{s1} (m/s)
1	14.6	24.7	85	44	238	276
2	3.6	6.1	54	37	147	171
3	10.8	18.2	79	42	225	261
4	4.5	7.4	56	38	160	186

Shear wave velocities were also measured for the compacted sand at depths of 1.5, 3.1, and 4.6 m. These velocities were intended to provide a secondary means of characterizing the in-place soil properties. In general, shear wave velocities for the loose sand were about 30–40% lower than that of the dense sand. Similar to the correction for CPT tip resistance, the measured shear wave velocity v_s was also corrected for the influence of overburden pressure. Using the procedure outlined by Robertson et al. (1992), the corrected shear wave velocity v_{s1} is given by $v_{s1} = v_s C_{vs}$, where $C_{vs} = \sqrt[4]{P_a / \sigma'_v}$ with $P_a = 0.1$ MPa and σ'_v = effective overburden pressure as before. The corrected shear wave velocities were 276 and 261 m/s for the dense sand and 171 and 186 m/s for the loose sand. Table 2 summarizes the in-place soil properties for the four tests, where q_c = average measured tip resistance, q_{c1} = average normalized tip resistance, D_r = relative density, $\bar{\phi}$ = friction angle, v_s = measured shear wave velocity, and v_{s1} = normalized shear wave velocity. Note that the shear wave velocity in Table 2 was based on the average value of four soundings per test.

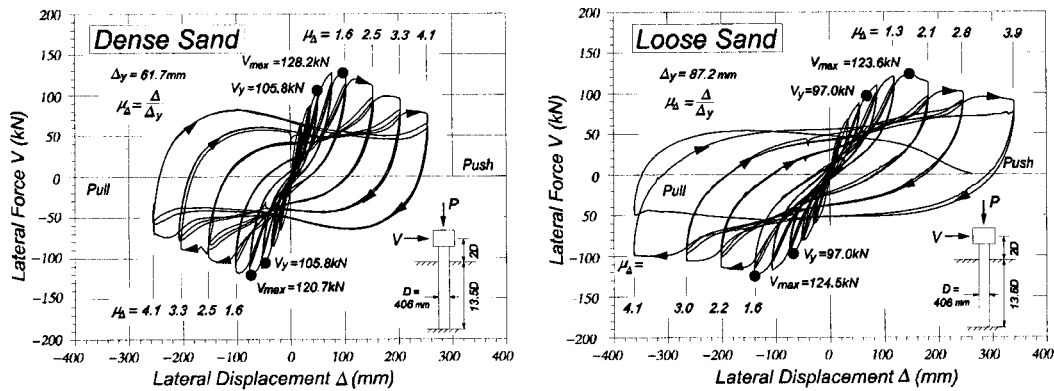


(a) Soil Gap and Final Failure of Piles with Above-Ground Height of 2D

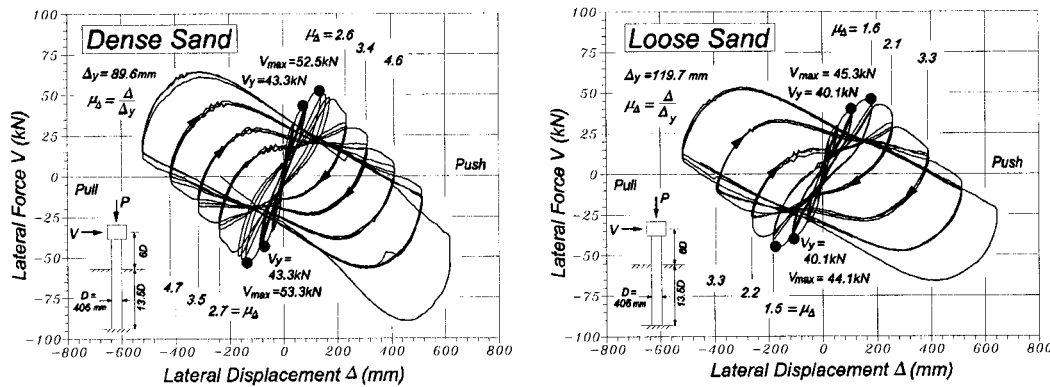


(b) Flexural Cracking and Final Failure of Piles with Above-Ground Height of 6D

Fig. 5. Deformation and failures of test piles



(a) Above-Ground Height = 2D



(b) Above-Ground Height = 6D

Fig. 6. Lateral force versus lateral displacement response of test piles

Observations and Results

Damage Characteristics of Test Piles

The lateral force or displacement imposed at the top of the pile resulted in a maximum bending moment and plastic hinge occurring below the ground level. The depth-to-maximum-moment, and hence the location of the plastic hinge, depends on the above-ground height and density of the soil, and these depths were found to vary from 1.25D to 3.3D. In general, a fairly large soil gap developed around the pile at relatively small lateral force. Minor flexural cracking was noted in the pile above the ground, particularly for the taller pile. Damage in the pile below ground, however, was generally difficult to observe during testing. After each test, the soil on one side of the pile was carefully excavated to allow an examination of the final pile damage. Despite the fairly low confining steel ratio in two of the test piles, ductile flexural failure was observed in all four tests with fracture of the transverse spiral noted in three of the four tests. Fig. 5 shows the deformation of the test pile during testing and the observed final pile damage after excavation. Details of the damage characteristics of test piles are described in Chai and Hutchinson (1999).

Lateral Force versus Lateral Displacement

The global response of the pile, as characterized by the lateral force versus lateral displacement hysteresis loops, is shown in Figs. 6(a and b) for the pile with aboveground heights of 2D and

6D, respectively. The lateral force on the y axis has been corrected for the horizontal component of the vertical force due to an interaction between the vertical and horizontal loading systems in the test setup. Note that the lateral displacement in Figs. 6(a and b) corresponds to the displacement at the point of lateral force application, i.e., at the top of the pile, and the displacement ductility factor μ_{Δ} has been defined in terms of an equivalent elastoplastic yield displacement Δ_y , which was determined by extrapolating the lateral displacement Δ'_y at the theoretical lateral yield force V_y to the maximum lateral force V_{max} . The theoretical lateral yield force V_y of the soil-pile system was estimated using the first-yield moment of the pile section while taking into account the confinement effect of the transverse reinforcement (Mander et al. 1988). The estimated first-yield lateral force V_y , measured maximum lateral force V_{max} , first-yield lateral displacement Δ'_y , elastoplastic yield displacement Δ_y , and secant lateral stiffness of the soil-pile system K_{sp} are summarized in Table 3.

Table 3. Summary of Soil-Pile Lateral Response

Pile No.	V_y (kN)	V_{max} (kN)	Δ'_y (mm)	Δ_y (mm)	K_{sp} (kN/m)	n_h (kN/m ³)
1	105.8	124.5	52.4	61.7	2018	9798
2	97.0	124.1	68.2	87.2	1423	4508
3	43.3	52.9	73.3	89.6	590	12333
4	40.1	44.7	107.3	119.6	374	2609

Note that the secant lateral stiffness of the soil-pile system K_{sp} has been defined using the first-yield limit state of the pile and is given by V_y/Δ'_y .

Test Piles with Aboveground Height of $2D$

The lateral force versus lateral displacement response of the pile with an aboveground height of $2D$ was relatively stable, as can be seen in Fig. 6(a). The lateral yield force was estimated to be $V_y = 105.8$ and 97.0 kN for the pile in dense and loose sands, respectively, and their corresponding elastoplastic yield displacements were $\Delta_y = 61.7$ and 87.2 mm. The maximum displacement imposed on the pile in dense sand was $\Delta_{max} = 253$ and -255 mm, which corresponded to a displacement ductility factor of $\mu_\Delta = 4.1$. During the first cycle to the maximum displacement, the pile in dense sand showed a 42% degradation of lateral strength compared to the peak horizontal force in the push direction and a 46% degradation of lateral strength in the pull direction. For the pile in loose sand, a larger lateral displacement of $\Delta_{max} = 340$ and -362 mm, or corresponding to a displacement ductility factor of $\mu_\Delta = 3.9$ and 4.1 , was imposed. Despite the larger lateral displacement, the pile in loose sand exhibited a lesser degradation of lateral strength in the first cycle to the maximum displacement, with approximately 28% and 21% degradation of lateral strength (compared to the peak force) in the push and pull directions, respectively. Note that the maximum horizontal force of the pile with an aboveground height of $2D$ was approximately equal for both dense and loose sands, even though the tip resistance of the loose sand was about 1/3 that of the dense sand. The maximum horizontal force was $V_{max} = 128.2$ and -120.7 kN for the pile in dense sand, whereas the maximum horizontal force was $V_{max} = 123.6$ and -124.5 kN for the pile in loose sand. The near equal maximum horizontal force of piles in dense and loose sands indicated that the lateral strength of the soil-pile system tended to be dominated by the flexural strength of the pile rather than by the strength of the soil.

Test Piles with Aboveground Height of $6D$

Fig. 6(b) shows the lateral force versus lateral displacement response of the pile in dense and loose sands with an aboveground height of $6D$. The increased flexibility of the pile due to a larger aboveground height showed a pronounced influence of $P-\Delta$ moment on the pile's lateral response. The effective lateral strength of the soil-pile system was significantly reduced by the presence of the secondary moment. The effective lateral yield force was estimated to be $V_y = 43.3$ kN for the pile in dense sand and $V_y = 40.1$ kN for the pile in loose sand. The experimental elastoplastic yield displacement, averaged for the two directions of loading, was $\Delta_y = 89.6$ mm for the pile in dense sand and $\Delta_y = 119.6$ mm for the pile in loose sand. For the pile in dense sand, the maximum lateral force was $V_{max} = 52.5$ and -53.3 kN, whereas the maximum lateral force for the pile in loose sand was $V_{max} = 45.3$ and -44.1 kN. These maximum lateral forces were measured at displacement ductility factors of $\mu_\Delta = 1.5$ for the pile in dense sand and at $\mu_\Delta = 1.6$ and 1.5 for the pile in loose sand. The significant influence of $P-\Delta$ moment on pile response can be seen by comparing the effective lateral force at different displacement ductility factors. For example, for the pile in dense sand, the lateral strength at $\mu_\Delta = 4.6$ was only 12% of the maximum lateral force, whereas for the pile in loose sand, the lateral strength at $\mu_\Delta = 3.3$ was 26% of the maximum lateral force.

The lateral force versus lateral displacement response of the pile with an aboveground height of $6D$ indicated a reversal in the direction of lateral force in the final few cycles, as can be seen in

Fig. 6(b). The lateral force reversed when the lateral displacement imposed by the actuator exceeded the limiting displacement permitted by the $P-\Delta$ moment. Such loading condition, however, was artificial since the actuator restrained the pile from further displacement, and hence prevented the pile from failure by overturning. The limiting displacement permitted by the $P-\Delta$ moment, however, can be estimated using the ultimate flexural strength of the pile and the axial force acting on the pile

$$\Delta_{lim} \approx \frac{M_p}{P} \quad (1)$$

where M_p = ultimate flexural strength of the pile and P = vertical force. Note that in estimating the limiting displacement by Eq. (1), the lateral resistance of the soil has been ignored. Substituting the flexural strength of the pile $M_p \approx 214$ kN m and vertical force $P = 445$ kN into Eq. (1), the limiting displacement is $\Delta_{lim} = 480$ mm for both piles with an aboveground height of $6D$. It can be seen from Fig. 6(b) that the calculated limiting displacement Δ_{lim} is very close to the displacement where the effective lateral force crosses over the horizontal axis for both dense and loose sand conditions.

Curvature Distribution in Piles

Of particular importance in the characterization of the inelastic response of piles is the magnitude of the local deformation upon formation of a plastic hinge. The local deformation can be characterized in terms of the curvature distribution along the length of the pile. Figs. 7(a and b) show the measured curvature distribution for all four test piles for displacement ductility factors from $\mu_\Delta = 1.2$ to 3.1 . Although the measured curvature distribution showed a considerable variation, the region of maximum flexural deformation was fairly well defined. It is worth noting that, upon integrating the curvature distribution in Figs. 7(a or b) twice, the resulting displacement was within 18% of the lateral displacement measured at the top of the pile. The technique for measuring the curvature distribution of piles below the ground level are discussed in Chai and Hutchinson (1999).

For the pile with an aboveground height of $2D$ and embedded in dense sand, the maximum curvature was measured at a depth of $2.4D$ even though the most severely damaged region of the pile occurred slightly deeper at a depth of $2.69D$. The maximum curvature was 154×10^{-3} rad/m and was measured at a displacement ductility factor of $\mu_\Delta = 2.7$. For the pile with an aboveground height of $2D$ and embedded in loose sand, the maximum curvature occurred at a depth of $3.4D$, which was very close to the most severely damaged region of the pile. The maximum curvature was 167×10^{-3} rad/m and was measured at a displacement ductility factor of $\mu_\Delta = 2.8$. Using an elastoplastic yield curvature of $\phi_y = 13.11 \times 10^{-3}$ rad/m, which was estimated from a moment-curvature analysis of the pile section, these curvatures corresponded to a curvature ductility factor of $\mu_\phi = 11.7$ and 12.7 for the pile in dense and loose sands, respectively. Thus the ratio of local curvature ductility factor to global displacement ductility factor was 4.3 for the pile in dense sand and 4.5 for the pile in loose sand. Note that the curvature distribution for the pile in loose sand showed a more gradual decrease of curvature with depth below the section of maximum curvature when compared to that of the pile in dense sand. The reduced stiffness of the loose soil enabled a larger spread of curvature below the section of maximum curvature.

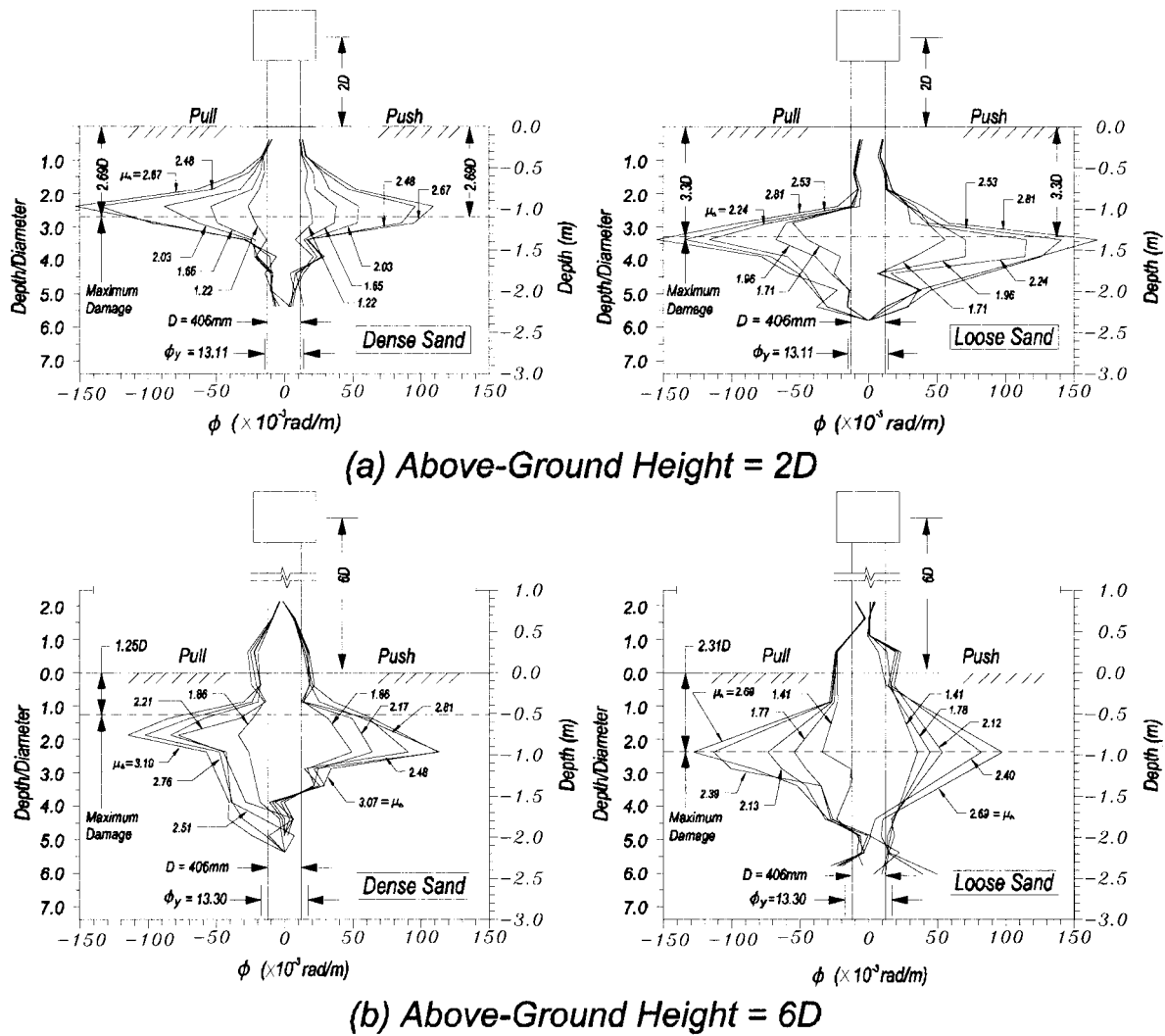


Fig. 7. Curvature distributions in test piles

For the pile with an aboveground height of 6D and embedded in dense sand, the maximum curvature was measured at a depth of 2.1D and was about 1D deeper than the depth where the most severely damaged region of the pile was observed. A maximum curvature of 114×10^{-3} rad/m was measured at a displacement ductility factor of $\mu_{\Delta} = 3.1$. For the pile with an aboveground height of 6D and embedded in loose sand, the maximum curvature occurred at a greater depth of 2.3D. This depth, however, agreed well with the depth where the most severely damaged region of the pile was noted. In this case, the maximum curvature was 128×10^{-3} rad/m and was measured at a displacement ductility factor of $\mu_{\Delta} = 3.0$. Using an elastoplastic yield curvature of $\phi_y = 13.30 \times 10^{-3}$ rad/m, these curvatures corresponded to a curvature ductility factor of $\mu_{\phi} = 8.6$ and 9.6 for the pile in dense and loose sands, respectively. Thus the ratio of curvature ductility factor to displacement ductility factor was 2.8 for the pile in dense sand and 3.2 for the pile in loose sand. It should be noted that the elastoplastic yield curvature of the pile with an aboveground height of 6D was slightly different from that of the pile with an aboveground height of 2D due to a different confining steel ratio and slightly different concrete compressive strength. It is also worth noting that the curvature distribution for the pile with an aboveground height of 6D was more gradual due to a smaller moment gradient, resulting in the curvature distribution

extending to a greater depth when compared to that of the test pile with an aboveground height of 2D.

Equivalent Plastic Hinge Length

An objective of the experimental program was to determine the equivalent plastic hinge length of the reinforced concrete pile when embedded in a soil medium. This can be achieved using the measured curvature distribution shown in Figs. 7(a and b). By assuming a concentrated plastic hinge rotation at the depth of maximum bending moment, the normalized plastic hinge length is given by Chai (2002)

$$\lambda_p \equiv \frac{L_p}{D} = \frac{\Delta_y(\mu_{\Delta} - 1)}{(L_a + L_m)(\mu_{\phi} - 1)\phi_y D} \quad (2)$$

where L_p = equivalent plastic hinge length; L_a = aboveground height; L_m = depth-to-maximum-moment; μ_{Δ} = displacement ductility factor; μ_{ϕ} = curvature ductility factor; ϕ_y = equivalent elastoplastic yield curvature; and Δ_y = equivalent elastoplastic yield displacement. Fig. 8 shows the normalized plastic hinge length λ_p versus the displacement ductility factor for $\mu_{\Delta} = 1.2 - 3.1$. The equivalent plastic hinge length was relatively constant with respect to the displacement ductility factor and was not very sensitive to the change in soil density. For the test pile with an above-

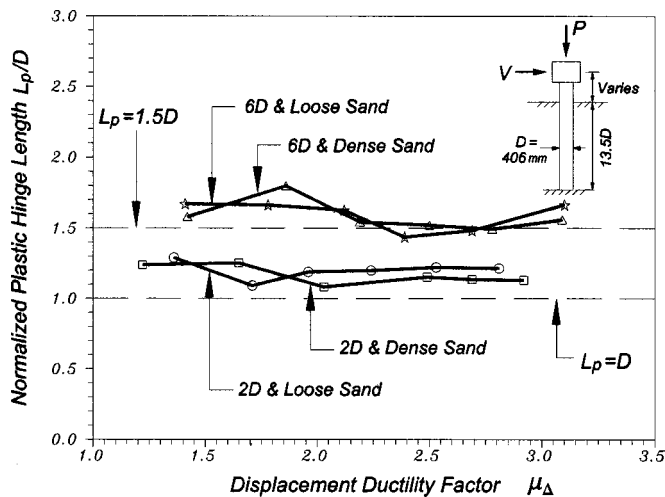


Fig. 8. Experimental equivalent plastic hinge length

ground height of $2D$, the equivalent plastic hinge length was about 20% larger than one pile diameter. The equivalent plastic hinge length, however, depended on the aboveground height. For the pile with an aboveground height of $6D$, the equivalent plastic hinge length was larger due to a smaller moment gradient, which in turn resulted in a more gradual distribution of curvature. In this case, the equivalent plastic hinge length averaged $1.58D$.

Horizontal Subgrade Reaction

The measured lateral stiffness of the soil-pile system K_{sp} , as summarized in Table 3, can be used to estimate the depth-to-fixity L_f of an equivalent fixed-base cantilever. By equating the lateral stiffness of the soil-pile system to the lateral stiffness of the cantilever, the rate of increase of horizontal subgrade reaction n_h can be estimated. The resulting value of n_h , which is also summarized in Table 3, is small relative to typical values recommended in the literature, e.g., ATC-32 (1996). The recommended value of n_h , however, should be interpreted as a value intended for working stress design where the lateral load level may be as low as 1/4 of the ultimate lateral strength. The definition of the yield limit state for the soil-pile system, on the other hand, should be based on first flexural yielding of the reinforcement in the pile (Chai 2002), which is only reached after a substantial deformation of the soil. Thus the value of n_h recommended for working stress design should be reduced when assessing the ductility capacity of the pile. From the limited data in this test program, 75% reduction in the value of n_h appears appropriate.

Comparison with Kinematic Model

Figs. 9(a–d) show the plot of measured curvature ductility factors and their comparisons with the curvature ductility factor simulated by the analytical model presented in Chai (2002). In simulating the local curvature ductility demand μ_ϕ , the value of n_h from Table 3 was used and the depth-to-maximum-moment was taken to be equal to the depth of the most severely damaged region of the pile. Equivalent plastic hinge lengths of $L_p = 1.2D$ and $L_p = 1.6D$ were used for the pile with aboveground heights of $2D$ and $6D$, respectively. It can be seen from Fig. 9 that the experimental curvature ductility factor μ_ϕ increases almost linearly with the displacement ductility factor μ_Δ . For the pile with an aboveground height of $2D$, the kinematic model underpredicts

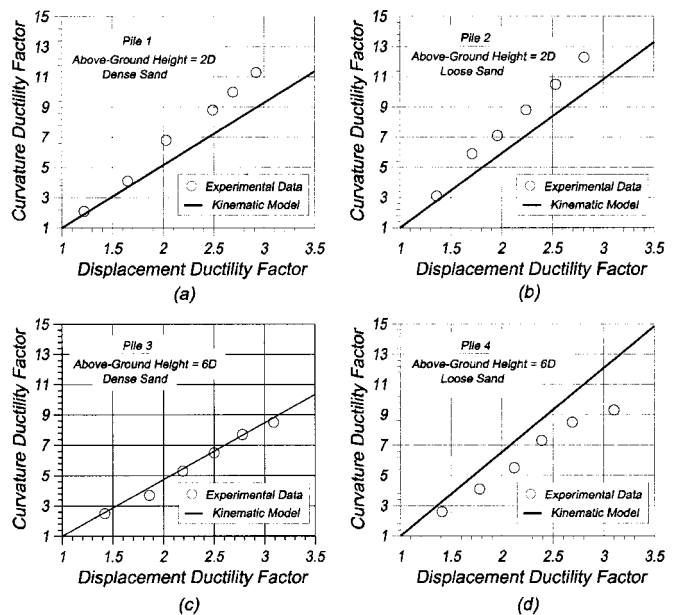


Fig. 9. Comparison between experimental and theoretical curvature ductility demand

the curvature ductility demand by about 20%, for both dense and loose sands. For the pile with an aboveground height of $6D$ and embedded in dense sand, the model provides a fairly good prediction of the curvature ductility demand up to a displacement ductility factor of $\mu_\Delta = 3.1$. For the pile with an aboveground height of $6D$ but embedded in loose sand, however, the model overpredicts the curvature ductility demand by about 24% at a displacement ductility factor of $\mu_\Delta = 2.7$ and by about 38% at a displacement ductility factor of $\mu_\Delta = 3.1$. As the simulation of local deformation in a reinforced concrete member is generally difficult, the estimation of local curvature ductility demand by the kinematic model seems fairly reasonable.

Conclusions

Current seismic design of bridges is based on an assumed ductile response of the structure. While the foundation system for many bridge structures may be designed to remain elastic with structural yielding limited to the aboveground portion of the structure, for bridge structures supported on extended pile-shafts, inelastic deformation of the pile-shaft below the ground level may not be avoidable during a severe earthquake. For performance evaluation of such structures, an assessment of the local ductility demand in the yielding pile-shaft is important.

Results of an experimental program to investigate the in-ground plastic hinging characteristics of reinforced concrete piles are presented in this paper. Four full-scale reinforced concrete piles with aboveground heights of $2D$ and $6D$, and embedded in loose and dense dry sand conditions, were tested under combined axial compression and reversed cyclic lateral displacement. Ductile flexural behavior was observed for all test piles despite a fairly low confining steel ratio in two of the test piles. Test results indicated that the lateral strength of the soil-pile system was not very sensitive to the soil density and was dominated by the flexural strength of the pile. The equivalent plastic hinge length, determined using curvatures measured along the length of the pile, indicated that the plastic hinge length varied between $1.2D$ and

1.6D and was not sensitive to the soil density or displacement ductility factor. However, the equivalent plastic hinge length increases with an increase in the aboveground height due to a more gradual distribution of bending moment in the taller pile.

The influence of $P-\Delta$ moment on the lateral force-displacement response of the pile may be significant for tall piles. Based on the observed response of the test pile with an aboveground height of 6D, instability failure may occur before fracture of the confining steel. Further research is, however, needed to characterize the influence of $P-\Delta$ moment on the lateral response of extended pile-shafts, particularly under dynamic conditions.

Acknowledgments

The research described in this paper was funded by Caltrans under Contract No. 59Y500 with Mr. Thomas Sardo as the Contract Monitor and Mr. Timothy Leahy as the Contract Manager. Their financial support is gratefully acknowledged. The valuable comments of Professor M. J. N. Priestley and Dr. Andy Budek, formerly of UC San Diego, and of Professor Ross Boulanger of UC Davis are appreciated. Any opinions, findings, and conclusions expressed in the paper are those of the writers and do not necessarily reflect the view of the sponsor.

References

Applied Technology Council ATC-32. (1996). *Improved seismic design criteria for California bridges: provisional recommendations*, Redwood City, Calif.

Banerjee, S., Stanton, J. F., and Hawkins, N. M. (1987). "Seismic per-

formance of precast prestressed concrete piles." *J. Struct. Eng.*, 113(2), 381–396.

Budek, A. M. (1997). "The inelastic behavior of reinforced concrete piles and pile shafts." PhD thesis, Univ. of California, San Diego.

Budek, A. M., Priestley, M. J. N., and Benzoni, G. (2000). "Inelastic seismic response of bridge drilled-shaft RC pile/columns." *J. Struct. Eng.*, 126(4), 510–517.

Chai, Y. H. (2002). "Flexural strength and ductility of extended pile-shafts. I: Analytical model." *J. Struct. Eng.*, 128(5), 586–594.

Chai, Y. H., and Hutchinson, T. C. (1999). "Flexural strength and ductility of reinforced concrete bridge piles." *Rep. No. UCD-STR-99-2*, Dept. of Civil and Environmental Engineering, UC Davis, Davis, Calif.

Liao, S. C., and Whitman, R. V. (1986). "Overburden correction factors for SPT in sand." *J. Geotech. Eng.*, 112(3), 373–377.

Mair, R. J., and Wood, D. M. (1987). *Pressuremeter testing*, Butterworths, London.

Mander, J. B., Priestley, M. J. N., and Park, R. (1988). "Theoretical stress-strain model for confined concrete." *J. Struct. Div., ASCE*, 114(8), 1804–1826.

Meyerhof, G. G. (1956). "Penetration tests and bearing capacity of cohesionless soils." *J. Soil Mech. Found. Div., Am. Soc. Civ. Eng.*, 82(SM1), 1–19.

Park, R., and Falconer, T. J. (1983). "Ductility of prestressed concrete piles subjected to simulated seismic loading." *PCI J.*, 28(5), 113–144.

Park, R. J. T., Priestley, M. J. N., and Berrill, J. B. (1987). "Seismic performance of steel-encased concrete piles." *Rep. No. 87-5*, Dept. of Civil Engineering, Univ. of Canterbury, N.Z.

Priestley, M. J. N., Seible, F., and Calvi, G. M. (1996). *Seismic design and retrofit of bridges*, Wiley-Interscience, New York.

Robertson, P. K., Woeller, D. J., and Finn, W. D. L. (1992). "Seismic cone penetration test for evaluating liquefaction potential under cyclic loading." *Can. Geotech. J.*, 29, 686–695.

Sheppard, D. A. (1983). "Seismic design of prestressed concrete piling." *PCI J.*, 28(2), 21–49.